Efficient Computation of Cross-Spectral Densities in the Stochastic Modelling of Waves and Wave Loads

Finn-Idar Grøtta Giske[a,b,*], Bernt Johan Leira[a], Ole Øiseth[c]

[a] *Department of Marine Technology, NTNU, 7491 Trondheim, Norway*
[b] *Multiconsult, Nedre Skøyen vei 2, 0213 Oslo, Norway*
[c] *Department of Structural Engineering, NTNU, 7491 Trondheim, Norway*

Abstract

A new method is presented for efficient calculation of auto- and cross-spectral densities in the stochastic modelling of ocean waves and wave loads. As part of the short-term response analyses, the method may contribute to more efficient long-term response prediction. Specifically the cross-spectral densities of the first order wave excitation forces are considered, but the method is straightforwardly generalized to other cross-spectral densities, e.g. for wave elevation, wave kinematics or second order loads. The method can be used with any choice of directional spreading function, but special attention is given to the commonly used *cos-2s* type directional distribution. In addition to the development of the new method, the traditional method using the trapezoidal rule for numerical quadrature is improved by developing an adaptive way of choosing the number of integration points. The accuracy of the adaptive method and the new method is investigated, revealing rapid convergence for both methods. However, the new method appears more robust as it avoids so-called spurious hat errors. When applied to two different pontoon type floating bridges the adaptive method and the new method both achieve a great improvement in computational effort compared to the traditional trapezoidal rule method. When the dimensions of the floating bridge increase, i.e. the number of pontoons and their relative distances increase, the new method is superior with respect to computation time.

Keywords: stochastic processes, wave excitation loads, directional waves, cross-spectral density, coherency, floating bridge

1. Introduction

For the assessment of extreme responses needed in the design of marine structures a full long-term response analysis is the most accurate approach [1, 2], and for fatigue design it is usually required [1, 3]. In the long-term approach

*Corresponding author
Email address: finn.i.giske@ntnu.no (Finn-Idar Grøtta Giske)

structural response analyses have to be carried out for a large number of sea states, which can be very time-consuming. Over the last decade new methods have been developed making long-term analysis more efficient, either by reducing the number of required short-term analyses [2, 4] or by computing the relevant short-term quantities more efficiently [5]. In the short-term response analysis of marine structures the auto- and cross-spectral densities of the wave load are important quantities, and their computation may contribute significantly to the computation time, for instance when the power spectral density method [6] is applied. The method proposed in this paper contributes to more efficient short-term analyses by making the evaluation of auto- and cross-spectral densities more efficient.

When the sea surface is modelled as a stochastic process the cross-spectral density between the wave elevations at the points (x_m, y_m) and (x_n, y_n) can be written as

$$S_{mn}(\omega) = \int_{-\pi}^{\pi} e^{i\kappa(\omega)L\cos(\beta-\theta)} S_{\eta\eta}^{(2)}(\theta,\omega)\, d\theta, \tag{1}$$

where $\kappa(\omega)$ is the wave number and $S_{\eta\eta}^{(2)}(\theta,\omega)$ denotes the directional wave spectrum [7]. β and L are constants that depend on the spatial separations $\Delta x = x_m - x_n$ and $\Delta y = y_m - y_n$, see Section 2.3 for definitions. In [8] a series expansion solution of the integral (1) is found by expressing the directional spectrum as a Fourier series and solving the integral term-by-term using Bessel functions, see also Section 7.2.1 of [7]. This series expansion is then used to obtain equations for the unknown Fourier coefficients of the directional spectrum such that these can be evaluated from measured cross-spectral densities. This paper deals with the reverse problem, as the aim is to evaluate the cross-spectral densities when a theoretical model for the directional spectrum is assumed.

A consistent stochastic theory of ocean waves and wave loading processes is presented in [9], which have been applied for offshore structures [10, 11] and floating bridges [6, 12, 13, 14, 15]. In this context calculation of the cross-spectral densities requires computation of integrals similar to (1), which can be written in the form

$$\int_{-\pi}^{\pi} f(\theta) e^{i\kappa(\omega)L\cos\theta} d\theta, \tag{2}$$

for some function $f(\theta)$. In applications these integrals have traditionally been evaluated using straightforward numerical quadrature [13, 15]. This requires care with respect to the number of integration points, because too few integration points may result in errors referred to as spurious hats [15]. The reason why these spurious hats occur is that when the factor $\kappa(\omega)L$ in (2) is large, the integral becomes highly oscillatory. It is worth mentioning that general methods for numerical quadrature of highly oscillatory integrals do exist [16, 17]. However, these methods are quite complex, especially for oscillatory integrals with stationary points like (2). Also, a more specialised computation method is expected to be more efficient.

In the present paper a new method is developed for the calculation of cross-spectral densities in the stochastic modelling of ocean waves and wave loads.

The series expansion solution of (1) found in [7, 8] is first generalized to the case of cross-spectral densities of first order wave excitation forces, and then utilized as a computational method for the cross-spectral densities. The method may readily be generalized to other cross-spectral densities, e.g. for wave elevation, wave kinematics or second order loads by using different transfer functions.

The new method will apply to any directional distribution expressed as a Fourier series. The Fourier coefficients of various theoretical models of the directional distribution can be found in [18] or in Section 2.5 of [19]. For the sake of completeness this paper includes a derivation of the Fourier coefficients of the *cos-2s* directional distribution in the most general case where s is any positive real number, thus providing a proof of the Fourier coefficients stated in [18, 19].

In addition to the development of the new method, the traditional method using the trapezoidal rule for numerical quadrature is improved by developing an adaptive way of choosing the number of integration points. This adaptive trapezoidal rule method is developed by observing when the spurious hats occur. The accuracy and efficiency is investigated for both the adaptive trapezoidal rule method and the new series expansion method. Finally the performances of the methods are compared when applied to pontoon type floating bridges.

2. Review of the stochastic modelling of ocean waves

2.1. Cross-spectral density

A common approach when modelling wind generated waves for engineering purposes is to assume that the sea elevation is a homogeneous stationary stochastic process [9]. The sea elevation at the point (x, y) at time t, denoted $\eta(x, y, t)$, is then written as

$$\eta(x, y, t) = \int_{-\infty}^{\infty} e^{i\omega t - i\kappa(x\cos\theta + y\sin\theta)} dB(\boldsymbol{\kappa}, \omega), \tag{3}$$

where $\boldsymbol{\kappa} = [\kappa\cos\theta, \kappa\sin\theta]$ is the wave number vector, ω is the frequency and $B(\boldsymbol{\kappa}, \omega)$ is the spectral process associated with the wave elevation. By further assuming the existence of a dispersion relation which relates the frequency ω and the wave number κ by a one-to-one mapping $\kappa = \kappa(\omega)$, or equivalently $\omega = \omega(\kappa)$, the cross-spectral density between the wave elevation at two points (x_m, y_m) and (x_n, y_n) can be expressed by

$$S_{mn}(\omega) = \int_{\theta} e^{-i\kappa(\omega)(\Delta x\cos\theta + \Delta y\sin\theta)} S^{(2)}_{\eta\eta}(\theta, \omega)\, d\theta,$$

where $\Delta x = x_m - x_n$ and $\Delta y = y_m - y_n$ is the separation of the locations (x_m, y_m) and (x_n, y_n) in space. $S^{(2)}_{\eta\eta}(\theta, \omega)$ is the directional wave spectral density. The details of the derivation is given in Appendix A as well as in [9]. According to the Airy wave theory, or linear wave theory, the dispersion relation takes the form

$$\omega^2 = \kappa g \tanh(\kappa d), \qquad \omega, \kappa \geq 0,$$

with water depth d and gravitational acceleration g, defining the function $\kappa(\omega)$ implicitly.

The directional wave spectral density $S^{(2)}_{\eta\eta}(\theta,\omega)$ is frequently written as $S^{(2)}_{\eta\eta}(\theta,\omega) = S_{\eta\eta}(\omega)\,\Psi(\theta,\omega)$ and thus separated into a one-dimensional wave spectral density $S_{\eta\eta}(\omega)$ and a spreading function $\Psi(\theta,\omega)$. The spreading function is sometimes assumed to be a function of the direction θ only, but such an assumption is not done here. For an overview of the various theoretical models for $S_{\eta\eta}(\omega)$ and $\Psi(\theta,\omega)$ see e.g. [19, 20]. The cross-spectral density can now be written as

$$S_{mn}(\omega) = S_{\eta\eta}(\omega)\int_{-\pi}^{\pi}\Psi(\theta,\omega)\,e^{-i\kappa(\omega)(\Delta x\cos\theta+\Delta y\sin\theta)}d\theta. \tag{4}$$

2.2. Auto-spectral density and complex coherency

If we consider the case $m = n$, we have that $\Delta x = \Delta y = 0$, and (4) gives an expression for the auto-spectral density

$$S_{nn}(\omega) = S_{\eta\eta}(\omega)\int_{-\pi}^{\pi}\Psi(\theta,\omega)\,d\theta. \tag{5}$$

Since the wave elevation is assumed to be homogeneous, the auto-spectral density should be equal to the one-dimensional wave spectral density at any point (x_n, y_n). This imposes the following normalization of the spreading function:

$$\int_{-\pi}^{\pi}\Psi(\theta,\omega)\,d\theta = 1. \tag{6}$$

The complex coherency is defined in terms of auto- and cross-spectral densities as

$$\gamma_{mn}(\omega) = \frac{S_{mn}(\omega)}{\sqrt{S_{nn}(\omega)S_{mm}(\omega)}}.$$

Combining equations (4), (5) and (6), we find that the complex coherency is given by

$$\gamma_{mn}(\omega) = \frac{S_{mn}(\omega)}{S_{\eta\eta}(\omega)} = \int_{-\pi}^{\pi}\Psi(\theta,\omega)\,e^{-i\kappa(\omega)(\Delta x\cos\theta+\Delta y\sin\theta)}d\theta. \tag{7}$$

The complex coherency is favourable to deal with in computations because it is dimensionless, independent of the one-dimensional spectral density and it satisfies $|\gamma_{mn}(\omega)| \leq 1$. For this reason most of the derivations in this paper will deal with the complex coherency rather than the cross-spectral density. The cross-spectral density can always be obtained from the complex coherency and the auto-spectral densities by

$$S_{mn}(\omega) = \gamma_{mn}(\omega)\sqrt{S_{nn}(\omega)S_{mm}(\omega)}.$$

2.3. Directional distribution function

The spreading function $\Psi(\theta,\omega)$ is commonly given as a distribution around a mean wave direction, in which case it is written as

$$\Psi(\theta,\omega) = D(\theta-\bar{\theta},\omega), \tag{8}$$

where $\bar{\theta}$ is the mean wave direction and $D(\phi,\omega)$ is the directional distribution function centred around zero. The directional distribution function is 2π-periodic and according to (6) it should integrate to one over one period. By inserting (8) into (7), using the periodicity of $D(\phi,\omega)$, the complex coherency can be expressed in terms of the directional distribution by

$$\gamma_{mn}(\omega) = \int_{-\pi}^{\pi} D(\phi,\omega)\, e^{-i\kappa(\omega)\left(\Delta x\cos\left(\phi+\bar{\theta}\right)+\Delta y\sin\left(\phi+\bar{\theta}\right)\right)} d\phi.$$

The linear combination of sine and cosine in the expression above can be written in terms of a single harmonic function as

$$-\Delta x\cos\left(\phi+\bar{\theta}\right)-\Delta y\sin\left(\phi+\bar{\theta}\right) = \sqrt{\Delta x^2+\Delta y^2}\cos\left(\phi+\bar{\theta}+\pi-\operatorname{atan2}\left(\Delta y,\Delta x\right)\right),$$

where $\operatorname{atan2}(\Delta y,\Delta x)$ is the generalization of $\arctan(\Delta y/\Delta x)$ that covers the entire circular range. If we then define

$$\begin{aligned} L &= \sqrt{\Delta x^2+\Delta y^2},\\ \beta &= \bar{\theta}+\pi-\operatorname{atan2}\left(\Delta y,\Delta x\right), \end{aligned}$$

we obtain

$$\gamma_{mn}(\omega) = \int_{-\pi}^{\pi} D(\phi,\omega)\, e^{i\kappa(\omega)L\cos(\phi+\beta)} d\phi = \int_{-\pi+\beta}^{\pi+\beta} D(\theta-\beta,\omega)\, e^{i\kappa(\omega)L\cos\theta} d\theta,$$

where the integrand is 2π-periodic. Thus the complex coherency is finally given as

$$\gamma_{mn}(\omega) = \int_{-\pi}^{\pi} D(\theta-\beta,\omega)\, e^{i\kappa(\omega)L\cos\theta} d\theta. \tag{9}$$

2.4. Series expansion of the complex coherency

Expressing the directional distribution function $D(\phi,\omega)$ as a Fourier series in ϕ, the integral (9) can be solved in terms of Bessel functions using the same approach as in [8], which is also given in Section 7.2.1 of [7].

Let the directional distribution function be given by the Fourier series

$$D(\phi,\omega) = \sum_{k=-\infty}^{\infty} c_k(\omega) e^{ik\phi}. \tag{10}$$

Since the directional distribution is a real function, the Fourier coefficients are required to satisfy $c_{-k}(\omega) = \overline{c_k(\omega)}$ for $k \geq 0$, the overline denoting complex

conjugation. Using this Fourier expansion in the expression (9) for the complex coherency yields

$$\gamma_{mn}(\omega) = \sum_{k=-\infty}^{\infty} c_k(\omega) e^{-ik\beta} \int_{-\pi}^{\pi} e^{ik\theta} e^{i\kappa(\omega)L\cos\theta} d\theta \tag{11}$$

where we have assumed that the order of summation and integration can be interchanged. The integrals in the above expression can be solved in terms of Bessel functions by utilizing the integral representation 9.1.21 in [21] stating that

$$J_k(z)\,\pi i^k = \int_0^{\pi} e^{iz\cos\theta} \cos(k\theta)\, d\theta,$$

where $J_k(z)$ is the Bessel function of the first kind with integer order k. Specifically we find that

$$\begin{aligned}\int_{-\pi}^{\pi} e^{ik\theta} e^{i\kappa(\omega)L\cos\theta} d\theta &= \int_{-\pi}^{\pi} e^{i\kappa(\omega)L\cos\theta} \cos(k\theta)\, d\theta + i\int_{-\pi}^{\pi} e^{i\kappa(\omega)L\cos\theta} \sin(k\theta)\, d\theta \\ &= 2\int_0^{\pi} e^{i\kappa(\omega)L\cos\theta} \cos(k\theta)\, d\theta \\ &= 2J_k(\kappa(\omega)L)\,\pi i^k,\end{aligned}$$

which inserted into (11) yields the following series expansion of the complex coherency:

$$\gamma_{mn}(\omega) = 2\pi \sum_{k=-\infty}^{\infty} c_k(\omega) i^k e^{-ik\beta} J_k(\kappa(\omega)L). \tag{12}$$

2.5. Directional distribution of the cos-2s type

The most commonly used directional distribution is given by

$$D(\phi,\omega) = \frac{2^{2s(\omega)}\Gamma^2(s(\omega)+1)}{2\pi\Gamma(2s(\omega)+1)} \cos^{2s(\omega)}\frac{\phi}{2}, \qquad \phi \in [-\pi,\pi), \tag{13}$$

where $\Gamma(\cdot)$ denotes the gamma function and $s(\omega)$ is a non-negative real valued function. This type of directional distribution was originally proposed by [22] and was developed further by [23] and [24] who investigated frequency dependence through the spreading parameter $s(\omega)$. Although in applications $s(\omega)$ is frequently assumed constant, wave data reveals a strong frequency dependence [18]. Throughout this paper the spreading parameter $s(\omega)$ is assumed to be a function of frequency. Note, however, that the ω-dependency will not be written explicitly as in (13) for simplicity of notation.

In order to make $D(\phi,\omega)$ as given by (13) a 2π-periodic function in ϕ for any $s \geq 0$, it should rather be written as

$$D(\phi,\omega) = \frac{2^{2s}\Gamma^2(s+1)}{2\pi\Gamma(2s+1)} \left(\cos^2\frac{\phi}{2}\right)^s, \qquad \phi \in \mathbb{R}. \tag{14}$$

If we rewrite $\cos^2\frac{\phi}{2} = \frac{1}{2}(1+\cos\phi)$ it is clear that this directional distribution is 2π-periodic. Writing $D(\phi,\omega)$ in this way rather than as in (13) will also ensure that $D(\phi,\omega)$ is real and non-negative at any ϕ for any choice of s. Now for an arbitrary non-negative real number s, the following identity holds according to Theorem 1 in Appendix B.

$$\left(\cos^2\frac{\phi}{2}\right)^s = \frac{1}{2^{2s}}\frac{\Gamma(2s+1)}{\Gamma^2(s+1)} + \frac{1}{2^{2s-1}}\sum_{k=1}^{\infty}\frac{\Gamma(2s+1)}{\Gamma(s-k+1)\,\Gamma(s+k+1)}\cos(k\phi), \tag{15}$$

Using this identity the directional distribution (14) can be written

$$\begin{aligned} D(\phi,\omega) &= \frac{1}{2\pi} + \frac{1}{\pi}\sum_{k=1}^{\infty}\frac{\Gamma^2(s+1)}{\Gamma(s-k+1)\,\Gamma(s+k+1)}\cos(k\phi) \\ &= \frac{1}{2\pi}\sum_{k=-\infty}^{\infty}\frac{\Gamma^2(s+1)}{\Gamma(s-k+1)\,\Gamma(s+k+1)}e^{ik\phi}, \end{aligned}$$

which is recognized as a Fourier series of the form (10) where

$$c_k(\omega) = \frac{1}{2\pi}\frac{\Gamma^2(s+1)}{\Gamma(s-k+1)\,\Gamma(s+k+1)}, \qquad k\in\{0,\pm1,\pm2,\ldots\}. \tag{16}$$

These Fourier coefficients agrees with those stated in [18, 19]. This derivation of the Fourier coefficients of the directional distribution (13) generalizes the derivation found in Section 7.2.1 of [7] which is valid for integer s.

3. Stochastic modelling of first order wave excitation loads

3.1. Exciting forces and moments on a rigid body

The hydrodynamic forces on a floating body can be decomposed into two parts, the wave excitation forces and the motion induced forces. We will now look at how the wave excitation forces can be modelled as a stochastic process. Consider a rigid body with a local coordinate system $(\tilde{x},\tilde{y})$ which is located with its origin at the point (x_0,y_0) and rotated counterclockwise with an angle α_0 relative to the global coordinate system (x,y) as shown in Figure 1. Thus (x_0,y_0) and α_0 specifies the location and orientation of the body. With this definition the global and local coordinates are related by

$$\begin{bmatrix} x \\ y \end{bmatrix} = \begin{bmatrix} x_0 + \tilde{x}\cos\alpha_0 - \tilde{y}\sin\alpha_0 \\ y_0 + \tilde{x}\sin\alpha_0 + \tilde{y}\cos\alpha_0 \end{bmatrix}. \tag{17}$$

Within the framework of linear potential theory, the hydrodynamic forces on a body of arbitrary shape can be computed using a panel method as implemented in software such as WAMIT[25] or WADAM[26]. The wave excitation forces are then reported in terms of the complex transfer function from the wave elevation

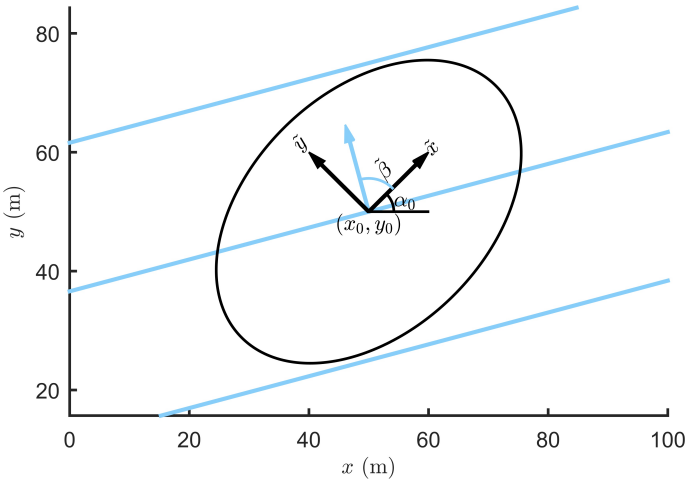

Figure 1: Local coordinate system of a rigid body and definition of wave propagation direction.

to the wave load. This means that for a regular incident wave of amplitude A given in local coordinates by

$$\eta(\tilde{x}, \tilde{y}, t) = A \exp\left\{ i\omega t - i\kappa \left(\tilde{x} \cos\tilde{\beta} + \tilde{y} \sin\tilde{\beta} \right) \right\}, \tag{18}$$

the forces and moments due to this wave will be given by $A\tilde{\mathbf{f}}_0(\tilde{\beta}, \omega)e^{i\omega t}$, where $\tilde{\mathbf{f}}_0(\tilde{\beta}, \omega)$ is the complex transfer function. Here $\tilde{\beta}$ is the wave propagation direction given as the angle relative to the $\tilde{x}$-axis, see Figure 1. The vector $\tilde{\mathbf{f}}_0$ contains six components, the transfer functions for three forces and three moments.

Provided the load due to any regular wave, the excitation load for the irregular wave (3) can be obtained by superposition. Inserting the relation (17) into (3) yields the sea elevation referring to the local coordinates of the body:

$$\eta\left(\tilde{x}, \tilde{y}, t\right) = \int_{-\infty}^{\infty} e^{i\omega t - i\kappa(\tilde{x}\cos(\theta-\alpha_0) + \tilde{y}\sin(\theta-\alpha_0))} e^{-i\kappa(x_0\cos\theta + y_0\sin\theta)} dB\left(\kappa, \omega\right). \tag{19}$$

Now since θ is the wave propagation direction relative to the global x-axis, we see from Figure 1 that $\alpha_0 + \tilde{\beta} = \theta$ which means that $\theta - \alpha_0$ can be identified as the local wave propagation direction $\tilde{\beta}$ in (18). Thus the first exponential in the above expression is recognized as the exponential of the incident wave (18). Hence (19) can be considered as a linear combination of (infinitely many) regular waves of amplitude $dB(\kappa, \omega)$ and, assuming the linear operations of calculating the wave load and taking the integral can be interchanged, we obtain an expression for the wave excitation load due to the irregular wave (3):

$$\tilde{\mathbf{q}}_0\left(t\right) = \int_{-\infty}^{\infty} \tilde{\mathbf{f}}_0\left(\theta - \alpha_0, \omega\right) e^{i\omega t - i\kappa(x_0\cos\theta + y_0\sin\theta)} dB\left(\kappa, \omega\right).$$

This expression gives the loads referring to the local coordinate system of the body, but the loads referring to the global coordinates are easily obtained by a

linear transformation

$$\mathbf{q}_0(t) = \mathbf{T}_0\tilde{\mathbf{q}}_0(t) = \int_{-\infty}^{\infty} \mathbf{f}_0(\theta - \alpha_0, \omega)\, e^{i\omega t - i\kappa(x_0\cos\theta + y_0\sin\theta)} dB(\kappa, \omega). \quad (20)$$

where $\mathbf{T}_0$ is the transformation matrix and $\mathbf{f}_0 = \mathbf{T}_0\tilde{\mathbf{f}}_0$.

3.2. Cross-spectral densities for wave excitation loads

We now consider the wave excitation loads for N bodies at the locations $(x_1, y_1), (x_2, y_2), \ldots, (x_N, y_N)$, with orientation angles $\alpha_1, \alpha_2, \ldots, \alpha_N$ relative to the global x-axis. The loads are conveniently organized into a total load vector

$$\mathbf{q} = \begin{bmatrix} \mathbf{q}_1^T & \mathbf{q}_2^T & \cdots & \mathbf{q}_N^T \end{bmatrix}^T.$$

Here $\mathbf{q}_n$ refers to the wave excitation loads on body number n which are given by (20) using the transfer function $\mathbf{f}_n$ corresponding to the body. Because each vector $\mathbf{q}_n$ contains six components, the total number of components in $\mathbf{q}$ will be $6N$. Each individual component can therefore be denoted by q_ν, where $\nu \in \{1, 2, \ldots, 6N\}$. Organizing the transfer functions $\mathbf{f}_n$ in the same manner, the individual loads are obtained from (20) as

$$q_\nu(t) = \int_{-\infty}^{\infty} f_\nu(\theta - \alpha_n, \omega)\, e^{i\omega t - i\kappa(x_n\cos\theta + y_n\sin\theta)} dB(\kappa, \omega). \quad (21)$$

The body number n corresponding to the index ν is given by $n = \lceil \nu/6 \rceil$, where $\lceil\cdot\rceil$ denotes the ceiling function giving the smallest integer not less than the argument.

Using the formulation (21) as starting point, the same derivation as in Section 2.1 can be carried out, yielding the cross-spectral density between the loads q_μ and q_ν as

$$\frac{S_{q_\mu q_\nu}(\omega)}{S_{\eta\eta}(\omega)} = \int_{-\pi}^{\pi} \Psi(\theta, \omega)\, f_\mu(\theta - \alpha_m, \omega)\overline{f_\nu(\theta - \alpha_n, \omega)} e^{-i\kappa(\omega)(\Delta x\cos\theta + \Delta y\sin\theta)} d\theta, \quad (22)$$

where the overline denotes complex conjugation.

3.3. Series expansion of the complex coherency

Using the same approach as in Section 2.3, the expression (22) for the cross-spectral density can be written as

$$\frac{S_{q_\mu q_\nu}(\omega)}{S_{\eta\eta}(\omega)} = \int_{-\pi}^{\pi} D(\theta - \beta, \omega) f_\mu\left(\theta - \beta + \bar{\theta} - \alpha_m, \omega\right)\overline{f_\nu\left(\theta - \beta + \bar{\theta} - \alpha_n, \omega\right)} e^{i\kappa L\cos\theta} d\theta. \quad (23)$$

Now the transfer functions are usually known only by their values at a finite number of heading angles. Then in order to perform the integration (23) we can use functions $f_\mu(\theta, \omega)$ that interpolates the transfer functions at the given values of the heading angle θ. For our purposes it is convenient to use trigonometric

interpolation [27, 28], which means that the transfer functions are given by trigonometric polynomials

$$f_\mu(\theta,\omega) = \sum_{k=-N_f}^{N_f} a_k^\mu(\omega)\, e^{ik\theta}. \tag{24}$$

If the transfer function values are given at heading angles uniformly distributed between 0 and 2π, the coefficients $a_k^\mu(\omega)$ can be efficiently computed using fast Fourier transform (FFT). If the number of heading angles is N_θ we have that $N_f = \lfloor N_\theta/2 \rfloor$.

With transfer functions given by (24) we find that

$$f_\mu\left(\phi+\bar\theta-\alpha_m,\omega\right) = \sum_{k=-N_f}^{N_f} \left(e^{ik\left(\bar\theta-\alpha_m\right)} a_k^\mu(\omega)\right) e^{ik\phi}$$

and

$$\begin{aligned}\overline{f_\nu\left(\phi+\bar\theta-\alpha_n,\omega\right)} &= \sum_{k=-N_f}^{N_f} \left(\overline{e^{ik\left(\bar\theta-\alpha_n\right)} a_k^\nu(\omega)}\right) e^{-ik\phi} \\ &= \sum_{k=-N_f}^{N_f} \left(\overline{e^{-ik\left(\bar\theta-\alpha_n\right)} a_{-k}^\nu(\omega)}\right) e^{ik\phi}.\end{aligned}$$

With a directional distribution given by (10) we have then available the individual Fourier series of each of the factors in the product $D(\phi,\omega) f_\mu\left(\phi+\bar\theta-\alpha_m,\omega\right)\overline{f_\nu\left(\phi+\bar\theta-\alpha_n,\omega\right)}$. It can be shown that the Fourier coefficients of a product can be obtained by taking the convolution of the Fourier coefficients of the factors. Thus we are able to find coefficients $C_k^{\mu\nu}(\omega)$ such that

$$D(\phi,\omega) f_\mu\left(\phi+\bar\theta-\alpha_m,\omega\right)\overline{f_\nu\left(\phi+\bar\theta-\alpha_n,\omega\right)} = \sum_{k=-\infty}^{\infty} C_k^{\mu\nu}(\omega)\, e^{ik\phi}. \tag{25}$$

Having the product $D(\phi,\omega) f_\mu\left(\phi+\bar\theta-\alpha_m,\omega\right)\overline{f_\nu\left(\phi+\bar\theta-\alpha_n,\omega\right)}$ developed as a Fourier series in ϕ makes the derivation of the series expansion (12) from Section 2.4 directly applicable. Inserting the Fourier expansion (25) into (23) yields the cross-spectral densities

$$S_{q_\mu q_\nu}(\omega) = 2\pi S_{\eta\eta}(\omega) \sum_{k=-\infty}^{\infty} C_k^{\mu\nu}(\omega) i^k e^{-ik\beta} J_k(\kappa(\omega)L). \tag{26}$$

In the special case that the Fourier series of the directional distribution is finite, it can be written as

$$D(\phi,\omega) = \sum_{k=-N_D}^{N_D} c_k(\omega)\, e^{ik\phi},$$

and the series expansion (26) will be finite. Specifically we have then that

$$S_{q_\mu q_\nu}(\omega) = 2\pi S_{\eta\eta}(\omega) \sum_{k=-N_{\text{tot}}}^{N_{\text{tot}}} C_k^{\mu\nu}(\omega) i^k e^{-ik\beta} J_k(\kappa(\omega)L),$$

where $N_{\text{tot}} = 2N_f + N_D$.

It is worth noticing that for the cross-spectral densities between loads at the same location we have that $m = n$ and thus $L = 0$. Using the fact that $J_k(0) = 0$ for $k \in \{\pm 1, \pm 2, \dots\}$ and $J_0(0) = 1$ yields the result

$$S_{q_\mu q_\nu}(\omega) = 2\pi S_{\eta\eta}(\omega) C_0^{\mu\nu}(\omega),$$

which holds whenever $m = n$, or equivalently $\lceil \mu/6 \rceil = \lceil \nu/6 \rceil$. The auto-spectral densities are thus given by

$$S_{q_\mu q_\mu}(\omega) = 2\pi S_{\eta\eta}(\omega) C_0^{\mu\mu}(\omega), \tag{27}$$

which gives the following formula for the complex coherencies:

$$\gamma_{q_\mu q_\nu}(\omega) = \frac{S_{q_\mu q_\nu}(\omega)}{\sqrt{S_{q_\mu q_\mu}(\omega) S_{q_\nu q_\nu}(\omega)}} = \sum_{k=-\infty}^{\infty} \frac{C_k^{\mu\nu}(\omega)}{\sqrt{C_0^{\mu\mu}(\omega) C_0^{\nu\nu}(\omega)}} i^k e^{-ik\beta} J_k(\kappa(\omega)L). \tag{28}$$

4. Computational methods for the complex coherencies

4.1. Approximation by the trapezoidal rule

By definition the complex coherencies are given by

$$\gamma_{q_\mu q_\nu}(\omega) = \frac{S_{q_\mu q_\nu}(\omega)}{\sqrt{S_{q_\mu q_\mu}(\omega) S_{q_\nu q_\nu}(\omega)}} = \frac{S_{q_\mu q_\nu}(\omega)/S_{\eta\eta}(\omega)}{\sqrt{S_{q_\mu q_\mu}(\omega)/S_{\eta\eta}(\omega)}\sqrt{S_{q_\nu q_\nu}(\omega)/S_{\eta\eta}(\omega)}}.$$

Inserting the expression (22) yields

$$\gamma_{q_\mu q_\nu}(\omega) = \frac{\int_{-\pi}^{\pi} \Psi(\theta,\omega) f_\mu(\theta - \alpha_m, \omega) \overline{f_\nu(\theta - \alpha_n, \omega)} e^{-i\kappa(\omega)(\Delta x \cos\theta + \Delta y \sin\theta)} d\theta}{\sqrt{\int_{-\pi}^{\pi} \Psi(\theta,\omega) |f_\mu(\theta - \alpha_m, \omega)|^2 d\theta \int_{-\pi}^{\pi} \Psi(\theta,\omega) |f_\nu(\theta - \alpha_n, \omega)|^2 d\theta}}. \tag{29}$$

We denote by $\widetilde{\gamma_{q_\mu q_\nu}}(\omega)$ the approximation obtained when the above expression is computed using the trapezoidal rule with $\tilde{N}$ integration points. Traditionally, the number of integration points $\tilde{N}$ is chosen to be the same for all values of μ, ν and ω, this will be referred to as the traditional trapezoidal rule method. As we will see the number of integration points should rather be adapted according to the value of ω, this will be referred to as the adaptive trapezoidal rule method.

We now consider two pontoons located at the points $(x_1, y_1) = (0, 0)$ and $(x_2, y_2) = (L, 0)$ with orientations $\alpha_1 = \alpha_2 = \pi/2$. The indices referring to the pontoon numbers are thus $m, n \in \{1, 2\}$ and the global indices are

$\mu, \nu \in \{1, 2, \ldots, 12\}$. The coherency matrix will then be a 12-by-12 matrix whose elements are $\gamma_{q_\mu q_\nu}(\omega)$. The transfer functions of the pontoons are evaluated by the software WADAM [26] at 36 different heading angles, so the transfer functions $f_\mu(\theta, \omega)$ are given by (24) with $N_f = 18$. The spreading function $\Psi(\theta, \omega)$ is given by a directional distribution of the *cos-2s* type as described in Section 2.5 with a constant spreading parameter $s(w) = s$. Note, however, that the methods described will be equally applicable for other directional distributions.

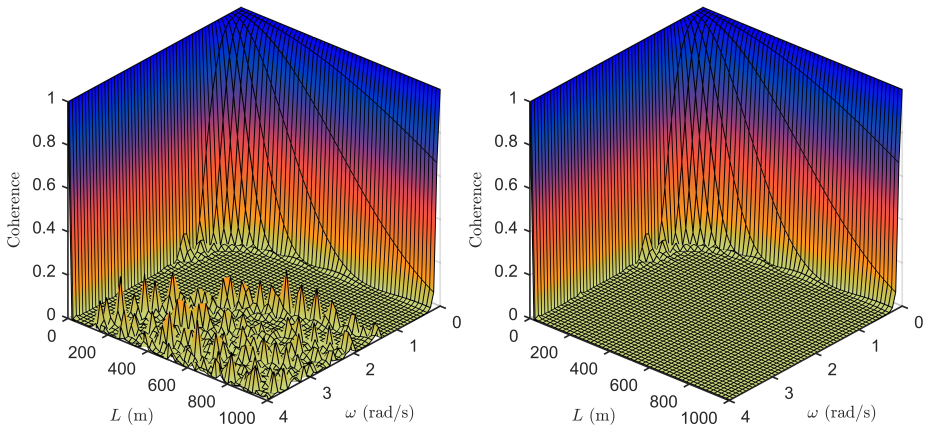

Figure 2: The coherence function $\left|\widetilde{\gamma_{q_1 q_7}}(\omega)\right|$ computed using the traditional trapezoidal rule method (29) for different distances L with spreading $s = 1$ and mean wave direction $\bar{\theta} = \pi/2$. The number of integration points are $\tilde{N} = 200$ (left) and $\tilde{N} = 1650$ (right).

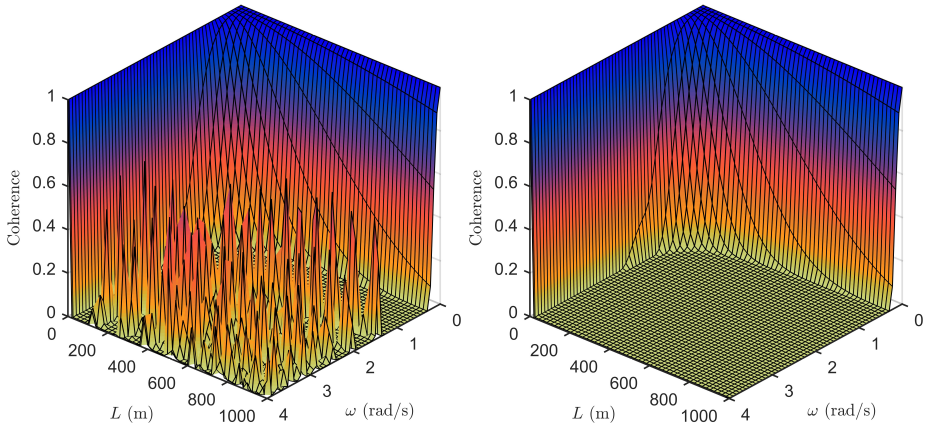

Figure 3: The coherence function $\left|\widetilde{\gamma_{q_1 q_7}}(\omega)\right|$ computed using the traditional trapezoidal rule method (29) for different distances L with spreading $s = 20$ and mean wave direction $\bar{\theta} = \pi/2$. The number of integration points are $\tilde{N} = 200$ (left) and $\tilde{N} = 1650$ (right).

Figure 2 and Figure 3 show the resulting coherence functions $\left|\widetilde{\gamma_{q_1 q_7}}(\omega)\right|$ when the complex coherency $\widetilde{\gamma_{q_1 q_7}}(\omega)$ is computed using the traditional trape-

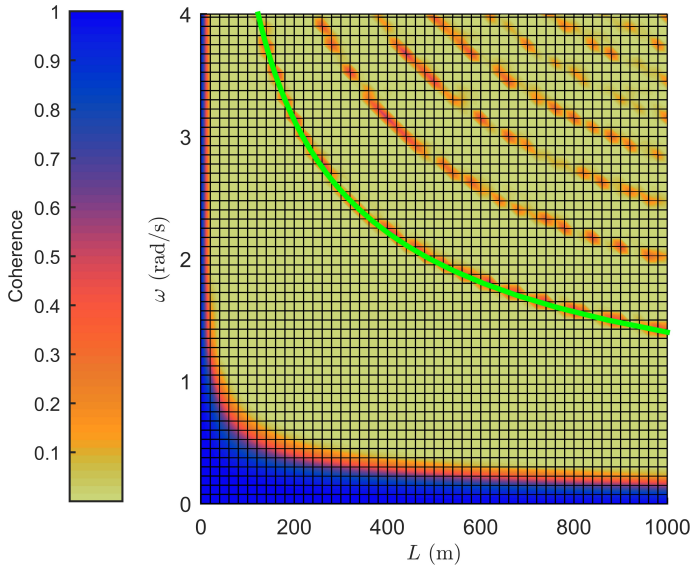

Figure 4: The coherence function $|\widetilde{\gamma_{q_1 q_7}}(\omega)|$ computed using the traditional trapezoidal rule method (29) with $\tilde{N} = 200$ integration points, along with the line defined by $\kappa(\omega)L = \tilde{N}$. The shading indicates the value of the coherence, identifying the spurious hats in the upper right corner.

zoidal rule method for different distances L between the pontoons. The mean wave direction is $\bar{\theta} = \pi/2$ and the spreading parameter is $s = 1$ in Figure 2, and $s = 20$ in Figure 3. Figure 2 and Figure 3 demonstrate that relatively large errors may occur if the number of integrations points $\tilde{N}$ is not large enough. These errors are the same as the spurious hats observed in [15]. The spurious hats can be explained by observing that the factor $\exp\{-i\kappa(\omega)(\Delta x \cos\theta + \Delta y \sin\theta)\}$ will make the upper integral in (29) highly oscillatory when the value of $\kappa(\omega)\sqrt{\Delta x^2 + \Delta y^2} = \kappa(\omega)L$ is large, and therefore the trapezoidal rule with $\tilde{N}$ integration points will be far too crude an approximation. Large values of $\kappa(\omega)$ occur when ω is large. When we consider $L \leq 1000$ m and $\omega \leq 4$ rad/s as in Figure 2 and Figure 3, we have that the maximal value of $\kappa(\omega)L$ is $(\kappa L)_{max} = 1631.5$. When the number of integration points $\tilde{N}$ is slightly larger than this, we observe that the spurious hats do not occur. Indeed if we plot the line defined by $\kappa(\omega)L = \tilde{N}$ along with the coherence function as in Figure 4 we see that the spurious hats starts occurring when the value of $\kappa(\omega)L$ becomes close to $\tilde{N}$. These observations suggest that the number of integration points used when calculating the coherency by the trapezoidal rule should be adapted according to the value of $\kappa(\omega)L$. This adaptive trapezoidal rule method is implemented in MATLAB [29] by calculating all the complex coherencies $\gamma_{q_\mu q_\nu}(\omega)$, $\mu, \nu = 1, 2, \ldots, 6N$, at each frequency ω using a number of integration points given by

$$\tilde{N} = \max\{\lceil \alpha(\kappa(\omega)L_{max}) \rceil, \tilde{N}_{min}\}, \tag{30}$$

where L_{max} is the maximal distance between any two pontoons and α is a factor determining the accuracy of the integration. The number $\tilde{N}_{min}$ is the number of integration points used when the value of $\kappa(\omega)L_{max}$ is small, meaning that the integrals are not highly oscillatory. In this paper the value $\tilde{N}_{min} = 100$ is used, but a larger value may be necessary if the transfer functions $f_\mu(\theta, \omega)$ are less well-behaved. With $\tilde{N}$ given by (30) the number of integration points is the same for all integrals at a given frequency. We could, however, choose $\tilde{N}$ according to the value of $\kappa(\omega)L$ for each individual integral. This is not done here because the former method allows for a faster implementation in MATLAB.

4.2. Approximation by the series expansion method

The new method proposed in this paper utilizes the series expansion (28) for computing the complex coherencies. If the directional distribution is given by a finite number of Fourier coefficients the series expansion will be finite as shown in Section 3.3 and the coherency matrix can be computed exactly. If the number of Fourier coefficients is infinite or excessively large, the complex coherencies can still be approximated by truncating the series expansion (28). The idea behind this approximation is that only the terms with index $|k| \leq \hat{N}$, for some number $\hat{N}$, will contribute to the total sum within the required precision. The complex coherencies are then approximated by

$$\widehat{\gamma_{q_\mu q_\nu}}(\omega) = \sum_{k=-\hat{N}}^{\hat{N}} \frac{C_k^{\mu\nu}(\omega)}{\sqrt{C_0^{\mu\mu}(\omega) C_0^{\nu\nu}(\omega)}} i^k e^{-ik\beta} J_k\left(\kappa(\omega)L\right). \tag{31}$$

This will be referred to as the series expansion method.

Figure 5 and Figure 6 show the resulting coherence functions $\left|\widehat{\gamma_{q_1 q_7}}(\omega)\right|$ when the complex coherency $\widehat{\gamma_{q_1 q_7}}(\omega)$ is computed using the series expansion method (31) for different distances L between the pontoons. The mean wave direction is $\bar{\theta} = \pi/2$ and the spreading parameter is $s = 1$ in Figure 5, and $s = 20$ in Figure 6. Since s is an integer we obtain the exact coherence functions using $\hat{N} = N_{tot} = 37$ for the case $s = 1$ and $\hat{N} = N_{tot} = 56$ for the case $s = 20$, see Section 3.3. Figure 5 and Figure 6 also indicate that when the complex coherency is approximated using the series expansion method with $\hat{N} < N_{tot}$ we obtain reasonable approximations even when $\hat{N}$ is quite small. Using (31) the coherence is approximated more smoothly, with no spurious hats, which is an appealing feature of this method.

4.3. The error of the approximation methods

In order to say something about the accuracy of the different ways to approximate the complex coherencies, we compare the exact coherency matrix obtained when the spreading parameter s is an integer with the coherency matrices obtained using the adaptive trapezoidal rule method and the series expansion method. The errors are measured by $\tilde{E} = \max_{\mu,\nu,\omega} \left|\gamma_{q_\mu q_\nu}(\omega) - \widetilde{\gamma_{q_\mu q_\nu}}(\omega)\right|$ and

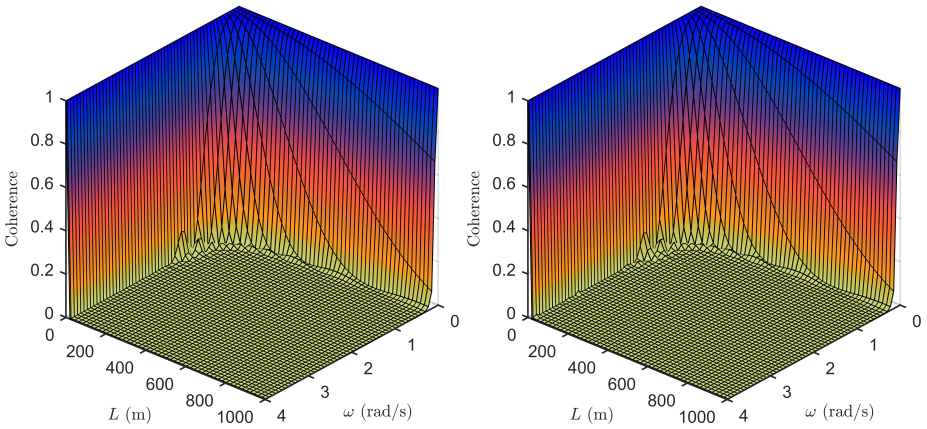

Figure 5: The coherence function $\left|\widehat{\gamma_{q_1 q_7}}(\omega)\right|$ computed using the series expansion method (31) for different distances L with spreading $s = 1$ and mean wave direction $\bar{\theta} = \pi/2$. The number of included terms are given by $\hat{N} = 5$ (left) and $\hat{N} = N_{tot} = 37$ (right).

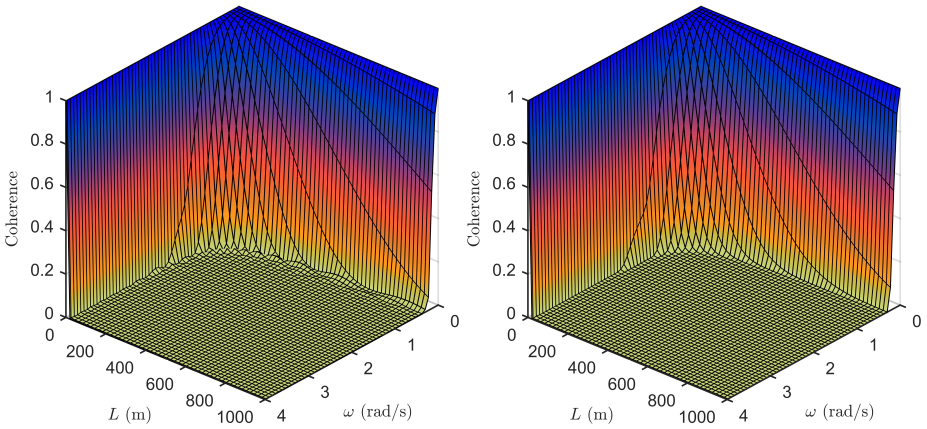

Figure 6: The coherence function $\left|\widehat{\gamma_{q_1 q_7}}(\omega)\right|$ computed using the series expansion method (31) for different distances L with spreading $s = 20$ and mean wave direction $\bar{\theta} = \pi/2$. The number of terms are given by $\hat{N} = 5$ (left) and $\hat{N} = N_{tot} = 56$ (right).

$\hat{E} = \max_{\mu,\nu,\omega} \left| \gamma_{q_\mu q_\nu}(\omega) - \widehat{\gamma_{q_\mu q_\nu}}(\omega) \right|$ for approximation by the adaptive trapezoidal rule and the series expansion respectively.

Figure 7 shows how the error $\tilde{E}$ of the adaptive trapezoidal rule method varies with the integration point parameter α in (30) for three different values of s and three different mean wave directions $\bar{\theta}$. We observe that the convergence is extremely fast as long as $\alpha > 1$, i.e. the number of integration points $\tilde{N}$ is larger than $\kappa(\omega)L$. This rapid convergence can be explained by the excellent convergence properties of the trapezoidal rule for periodic functions. Since we are using trigonometric interpolation for the transfer functions, the integrand will be infinitely many times continuously differentiable for integer s and geometric convergence is achieved [30]. We also observe a faster convergence when $\bar{\theta} = 0$ with increasing effect as s gets larger. This happens because for large s the directional distribution $D(\theta, \omega)$ will be practically zero except for a small band around $\theta = 0$, thus cancelling the rapid oscillations of the exponential factor when $\bar{\theta} = 0$.

Figure 8 shows how the error $\hat{E}$ of the series expansion method varies with $\hat{N}$ for three different values of s and three different mean wave directions $\bar{\theta}$. We see that it is not necessary to use all the available coefficients in order to get a good approximation, especially for larger values of s.

For non-integer values of s the *cos-2s* directional distribution will not have a finite Fourier series and we will not have an exact formula for the complex coherencies. However, by including only the Fourier coefficients (16) that are larger than e.g. 10^{-16} in absolute value we should obtain the exact solution up to round-off errors. Thus we can calculate the errors $\tilde{E}$ and $\hat{E}$ of the two methods like before. Figure 9 shows how the error $\tilde{E}$ of the adaptive trapezoidal rule method varies with the integration point parameter α for $\bar{\theta} = \pi/2$ and different non-integer values of s. When s is not an integer the directional distribution will no longer be infinitely many times continuously differentiable and the rapid convergence demonstrated in Figure 7 is no longer guaranteed. However, it appears that the error behaves the same as for integer valued s up to a certain point, and we see from Figure 9 that for $s > 4$ we have rapid convergence until round-off error dominates like before. Figure 10 shows how the error $\hat{E}$ of the series expansion method varies with $\hat{N}$ for $\bar{\theta} = 0$ and different non-integer values of s. Again we see that the convergence is slow for small values of s. This can be explained by observing that the Fourier coefficients (16) of the directional distribution approaches zero very fast for large enough s but more and more slowly as s decreases.

5. Wave excitation loads on pontoon type floating bridges

The cross-spectral density matrix of wave excitation loads is often needed as input for dynamic response analysis of floating bridges, both in the frequency and time domain [6, 12, 14]. For time domain analyses simulated realizations of the wave loading process can be obtained from the cross-spectral density matrix using the method found in [31]. An approach for modelling the stochastic

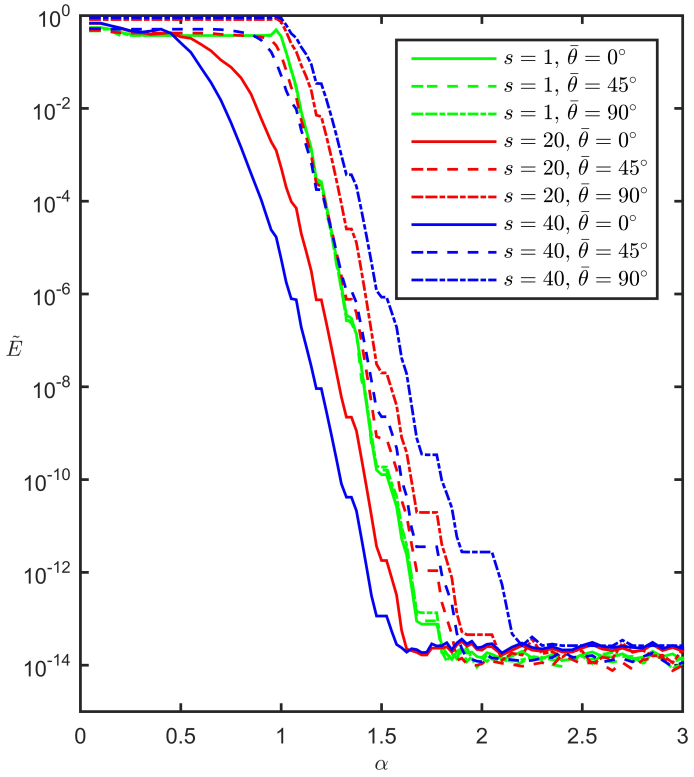

Figure 7: The error $\tilde{E}$ of the adaptive trapezoidal rule method as a function of the integration point parameter α in (30) for different values of the spreading s and the mean wave direction $\bar{\theta}$.

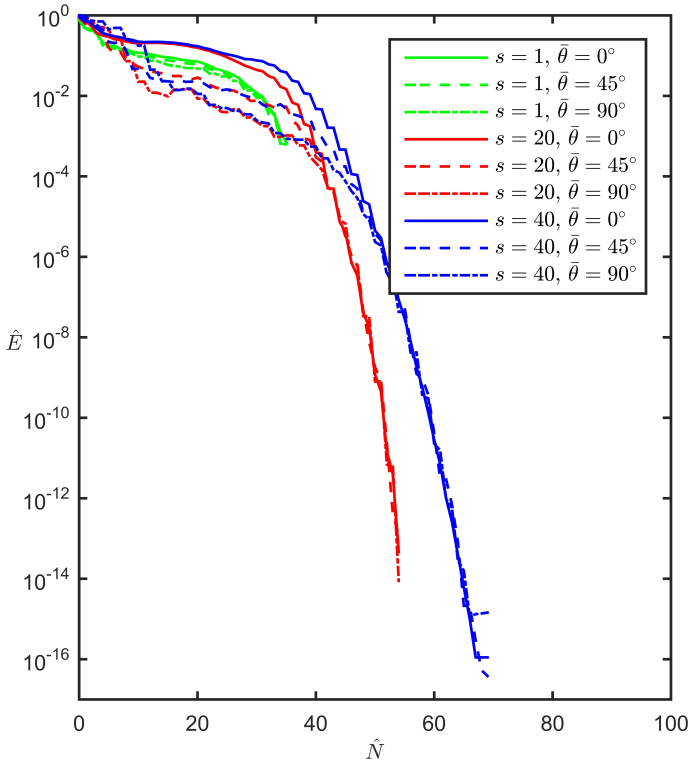

Figure 8: The error $\hat{E}$ of the series expansion method as a function of the number $\hat{N}$ of included terms in (31) for different values of the spreading s and the mean wave direction $\bar{\theta}$.

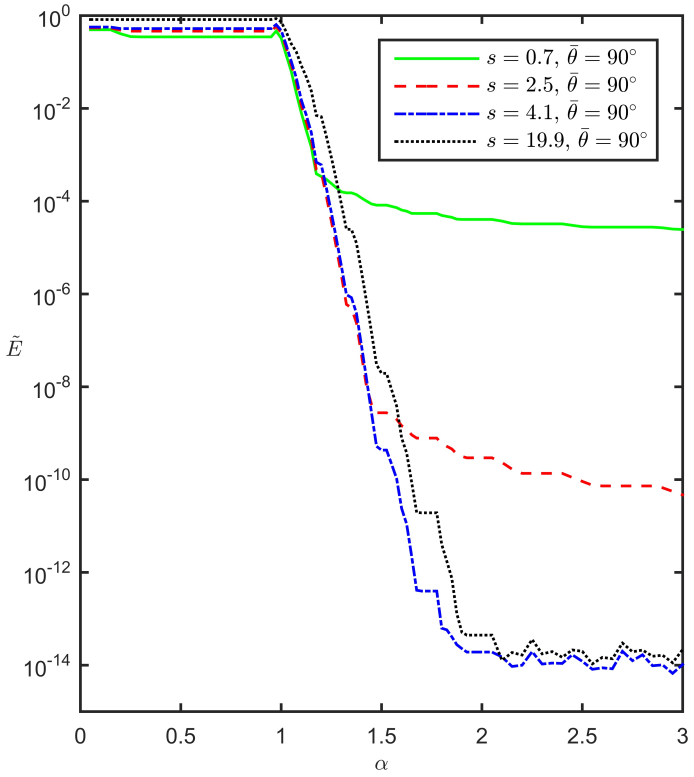

Figure 9: The error $\tilde{E}$ of the adaptive trapezoidal rule method as a function of the integration point parameter α for the mean wave direction $\bar{\theta} = \pi/2$ and different non-integer values of the spreading s.

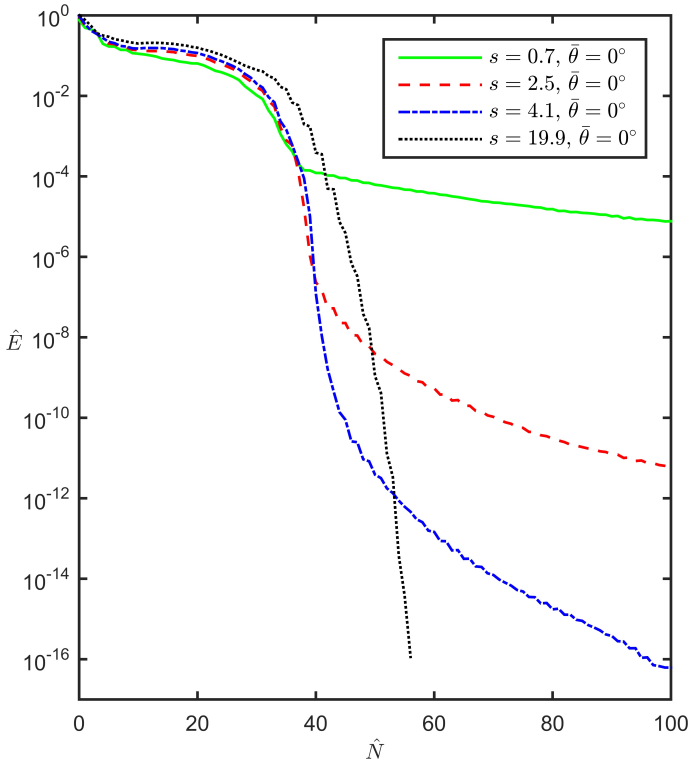

Figure 10: The error $\hat{E}$ of the series expansion method as a function of the number $\hat{N}$ of included terms in (31) for the mean wave direction $\bar{\theta} = 0$ and different non-integer values of the spreading s.

dynamic behaviour of pontoon type floating bridges is discussed in [6], where the structural response of the bridge is calculated in the frequency domain using the equation

$$\mathbf{S_u}(\omega) = \mathbf{H}(\omega)\,\mathbf{S_q}(\omega)\,\mathbf{H}(\omega)^H,$$

with superscript H denoting the conjugate transpose. Here $\mathbf{S_u}(\omega)$ and $\mathbf{S_q}(\omega)$ are the cross-spectral density matrices of the response $\mathbf{u}(t)$ and the wave excitation load $\mathbf{q}(t)$ respectively. $\mathbf{H}(\omega)$ is the transfer function matrix which takes into account the structural mass, damping and stiffness of the bridge structure, as well as hydrostatic stiffness, added mass and added damping due to the pontoons. The method proposed in this paper can be used to efficiently calculate the cross-spectral density matrix $\mathbf{S_q}(\omega)$ needed in this approach.

In the case of pontoon type floating bridges the structure will experience wave loads only where the pontoons are located, each pontoon is considered a rigid body and is thus loaded in six degrees of freedom (dofs). This means that with N pontoons the cross-spectral density matrix $\mathbf{S_q}(\omega)$ of the wave excitation loads will be a $6N$-by-$6N$ matrix whose elements are the cross-spectral densities $S_{q_\mu q_\nu}(\omega)$. The calculation of the cross-spectral density matrix must be performed for every wave situation considered, which in applications such as long-term response analyses can be a very large amount [2]. This motivates the need for an efficient calculation method.

In order to get some idea of how the different approximation methods perform with respect to computation time, the cross-spectral density matrix is computed for two different pontoon type floating bridges, the Bergsøysund bridge with $N = 7$ pontoons and a chained floating bridge with $N = 18$ pontoons [32]. The chained floating bridge is illustrated in Figure 11. The same pontoon type is used for both bridges, but the number of pontoons and their locations are different. The locations of the pontoons are shown in Figure 12 and Figure 13 for the Bergsøysund bridge and the chained floating bridge respectively. An example of a transfer function calculated using WADAM is given in Figure 14. The transfer functions are calculated for single pontoons, thus neglecting interaction effects among multiple bodies. This is justified by to the fact that the distance between pontoons is large compared to the dimensions of the pontoons. The cross-spectral density matrix is computed by first calculating all $(6N)^2$ coherencies $\gamma_{q_\mu q_\nu}(\omega)$ with an approximation error less than 10^{-3} as measured by $\tilde{E}$ and $\hat{E}$, see Section 4.3. Then the auto-spectral densities $S_{q_\nu q_\nu}(\omega)$ are calculated using (27) and the cross-spectral densities are found by the relation

$$S_{q_\mu q_\nu}(\omega) = \gamma_{q_\mu q_\nu}(\omega)\sqrt{S_{q_\mu q_\mu}(\omega)\,S_{q_\nu q_\nu}(\omega)}.$$

In this example the *cos-2s* directional distribution from Section 2.5 is used with a constant spreading parameter $s(\omega) = s$, and the one-dimensional wave spectral density $S_{\eta\eta}(\omega)$ is given by the Pierson-Moskowitz spectrum [20].

The approximation methods discussed in this paper are implemented in MATLAB and the computation times for the cases $s = 1$ and $s = 20$ are given in Table 1. Since the runtime in MATLAB is very sensitive to the specific

implementation, it is emphasized that the numbers in Table 1 are only meant to give some idea of the computational effort. It is clear, however, that the adaptive trapezoidal rule method and the series expansion method both achieve a great improvement in computational time, as compared to the traditional trapezoidal rule method. We also notice that the increase in computational effort due to larger distances between pontoons is much smaller for the series expansion method. In Table 1 we see that for the trapezoidal rule methods the computational time increases by a factor of approximately 100, while for the series expansion method the increase is only by a factor of approximately 6.

It should be pointed out that in many practical applications the cross-spectral densities between points at large distances are practically zero, making it a reasonable approximation to set them equal to zero. This will of course greatly improve the computation time and the trapezoidal rule methods may still be feasible. However, an assessment of whether this approximation is reasonable must then be carried out for each particular case. The new method proposed in this paper eliminates the need for such an assessment.

Figure 11: Chained floating bridge, illustration by Multiconsult.

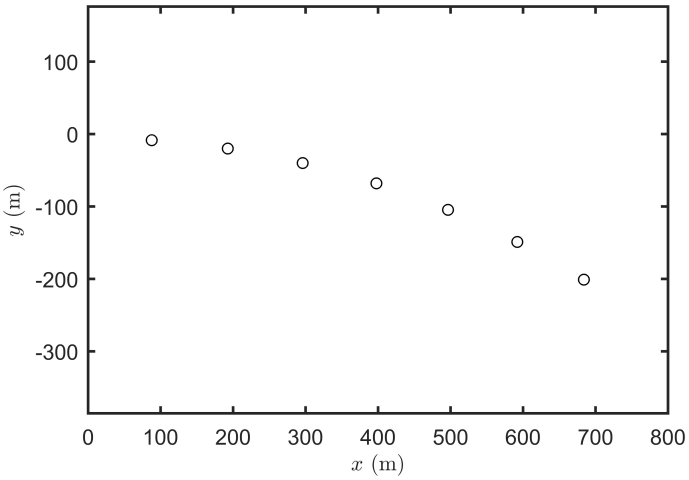

Figure 12: Pontoon locations for the Bergsøysund floating bridge.

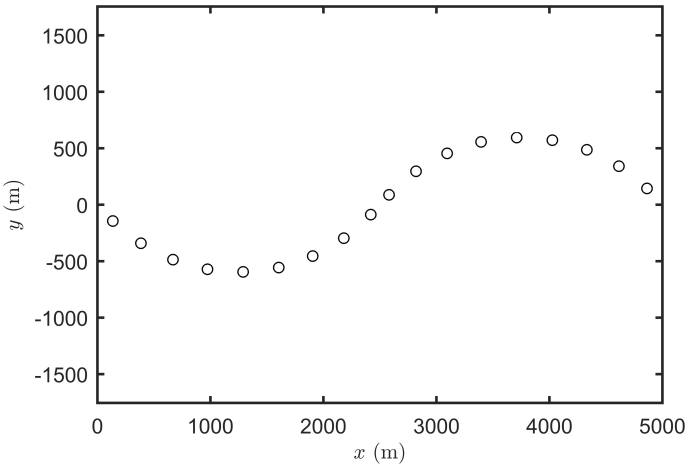

Figure 13: Pontoon locations for the chained floating bridge.

Table 1: The computation time for the different methods of calculating the cross-spectral density matrix. L_{max} is the maximal distance between two pontoons.

	$s = 1$	$s = 20$
Bergsøysund bridge – 7 pontoons, L_{max} = 626 m		
Traditional trapezoidal rule method	5.0 s	5.1 s
Adaptive trapezoidal rule method	1.5 s	1.6 s
Series expansion method	1.1 s	1.1 s
Chained floating bridge – 18 pontoons, L_{max} = 4735 m		
Traditional trapezoidal rule method	576 s	595 s
Adaptive trapezoidal rule method	171 s	176 s
Series expansion method	6.8 s	7.1 s

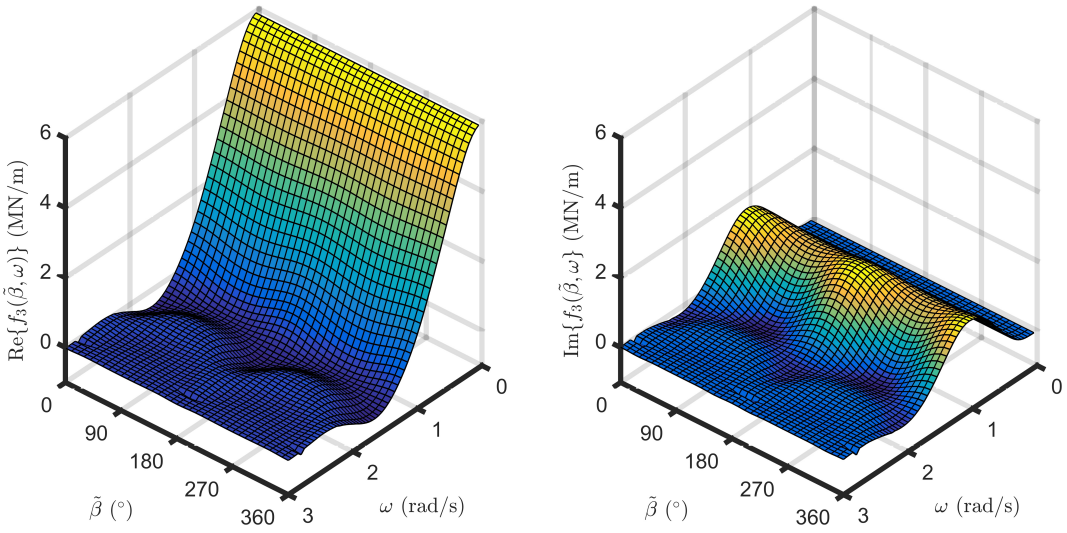

Figure 14: The transfer function for the heave force (vertical direction) on one pontoon, given by its real part (left) and imaginary part (right).

6. Conclusions

A new method has been presented for the calculation of cross-spectral densities in the stochastic modelling of ocean waves and wave loads, based on a series expansion solution of the integral expressing the cross-spectral density. The method is developed for first order wave excitation loads but it is readily extended to the computation of other cross-spectral densities, e.g. for wave elevation, wave kinematics or second order load. The only difference will be which transfer functions that are used. In addition to presenting the new method, the traditional trapezoidal rule method has been improved by developing an adaptive way of choosing the number of integration points.

The accuracy of the adaptive trapezoidal rule method and the series expansion method has been investigated. The adaptive trapezoidal rule method shows very rapid convergence after a certain point, before which the error is relatively large due to so-called spurious hats. The series expansion method also displays a generally rapid convergence, in addition to avoiding the spurious hat errors altogether.

When applied to two different pontoon type floating bridges the adaptive trapezoidal rule method and the series expansion method both achieve a great improvement in computational effort compared to the traditional trapezoidal rule method. When the dimensions of the floating bridge increase, i.e. the number of pontoons and their relative distances increase, the series expansion method is superior with respect to computation time.

Acknowledgements

The authors are grateful for grants which are provided by Multiconsult ASA and the Research Council of Norway.

References

[1] Naess A, Moan T. Stochastic Dynamics of Marine Structures. Cambridge: Cambridge University Press; 2012. ISBN 9781139021364. URL: http://ebooks.cambridge.org/ebook.jsf?bid=CBO9781139021364. doi:10.1017/CBO9781139021364.

[2] Sagrilo L, Naess A, Doria A. On the long-term response of marine structures. Appl Ocean Res 2011;33(3):208–14. URL: http://www.sciencedirect.com/science/article/pii/S0141118711000204. doi:10.1016/j.apor.2011.02.005.

[3] Low YM, Cheung SH. On the long-term fatigue assessment of mooring and riser systems. Ocean Eng 2012;53:60–71. URL: http://www.sciencedirect.com/science/article/pii/S0029801812002211. doi:10.1016/j.oceaneng.2012.06.017.

[4] Vázquez-Hernández A, Ellwanger G, Sagrilo L. Long-term response analysis of FPSO mooring systems. Appl Ocean Res 2011;33(4):375–83. URL: http://www.sciencedirect.com/science/article/pii/S0141118711000472. doi:10.1016/j.apor.2011.05.003.

[5] Naess A, Gaidai O, Teigen P. Extreme response prediction for nonlinear floating offshore structures by Monte Carlo simulation. Appl Ocean Res 2007;29(4):221–30. URL: http://www.sciencedirect.com/science/article/pii/S0141118708000035. doi:10.1016/j.apor.2007.12.001.

[6] Kvåle KA, Sigbjörnsson R, Øiseth O. Modelling the stochastic dynamic behaviour of a pontoon bridge: A case study. Comput Struct 2016;165:123–35. URL: http://www.sciencedirect.com/science/article/pii/S004579491500334X. doi:10.1016/j.compstruc.2015.12.009.

[7] Ochi MK. Ocean Waves. Cambridge: Cambridge University Press; 1998. ISBN 9780511529559. URL: http://ebooks.cambridge.org/ebook.jsf?bid=CBO9780511529559. doi:10.1017/CBO9780511529559.

[8] Panicker N, Borgman L. DIRECTIONAL SPECTRA FROM WAVE-GAGE ARRAYS. In: Coastal Engineering Proceedings; vol. 1. 1970, p. 117–36. URL: https://journals.tdl.org/icce/index.php/icce/article/view/2612.

[9] Sigbjörnsson R. Stochastic theory of wave loading processes. Eng Struct 1979;1(2):58–64. URL: http://www.sciencedirect.com/science/article/pii/0141029679900142. doi:10.1016/0141-0296(79)90014-2.

[10] Sigbjörnsson R, Smith EK. Wave induced vibrations of gravity platforms: a stochastic theory. Appl Math Model 1980;4(3):155–65. URL: http://www.sciencedirect.com/science/article/pii/0307904X80901250. doi:10.1016/0307-904X(80)90125-0.

[11] Sigbjörnsson R. Extreme and fatigue response of offshore platforms due to three-dimensional stochastic wave fields. Eng Struct 1981;3(4):219–24. URL: http://www.sciencedirect.com/science/article/pii/0141029681900043. doi:10.1016/0141-0296(81)90004-3.

[12] Kvåle KA, Øiseth O, Sigbjörnsson R. Modelling of the stochastic dynamic behaviour of the Bergsøysund Bridge: an application of the power spectral density method. In: IX International Conference on Structural Dynamics, EURODYN 2014; vol. 1. ISBN 9789727521654; 2014, p. 2921–8. URL: http://paginas.fe.up.pt/~eurodyn2014/CD/papers/406_MS16_ABS_1301.pdf.

[13] Georgiadis C, Hartz BJ. Wave coherence along continuous structures for directional spectral models. Tech. Rep.; SINTEF; Trondheim; 1982. URL: http://www.runet-software.com/documents/Wavecoherence.pdf.

[14] Langen I, Sigbjörnsson R. On stochastic dynamics of floating bridges. Eng struct 1980;2(4):209–16. URL: http://www.sciencedirect.com/science/article/pii/0141029680900024. doi:10.1016/0141-0296(80)90002-4.

[15] Langen I. Frequency Domain Analysis of a Floating Bridge Exposed to Irregular Short-crested Waves. Tech. Rep.; SINTEF; Trondheim; 1980.

[16] Olver S. Fast, numerically stable computation of oscillatory integrals with stationary points. BIT Numer Math 2010;50(1):149–71. URL: http://link.springer.com/10.1007/s10543-010-0251-y. doi:10.1007/s10543-010-0251-y.

[17] Iserles A. On the numerical quadrature of highly-oscillating integrals II: Irregular oscillators. IMA J Numer Anal 2005;25(1):25–44. URL: http://imajna.oxfordjournals.org/content/25/1/25. doi:10.1093/imanum/drh022.

[18] Krogstad HE, Barstow SF. Directional Distributions In Ocean Wave Spectra. In: The Ninth International Offshore and Polar Engineering Conference. International Society of Offshore and Polar Engineers; 1999, p. 79–86. URL: https://www.onepetro.org/conference-paper/ISOPE-I-99-237.

[19] Hauser D, Kahma K, Krogstad H. Measuring and analysing the directional spectra of ocean waves. Luxembourg: Publications Office of the European Union; 2005. ISBN 92-898-0003-8. URL: http://www.envia.bl.uk/handle/123456789/4300.

[20] Stansberg CT, Contento G, Hong SW, Irani M, Ishida S, Mercier R, et al. The Specialist Committee on Waves Final Report and Recommendations to the 23rd ITTC. In: Proceedings of the 23rd ITTC. 2002, p. 505–736. URL: http://ittc.info/downloads/Proceedings/23rdConference(Venice2002)/Waves.pdf.

[21] Abramowitz M, Stegun I. Handbook of Mathematical Functions with Formulas, Graphs, and Mathematical Tables. U.S. Department of Commerce, NIST; 1972. URL: http://app.knovel.com/hotlink/toc/id:kpHMFFGMT1/handbook-mathematical/handbook-mathematical.

[22] Longuet-Higgins M, Cartwright D, Smith N. Observations of the directional spectrum of sea waves using the motions of a floating buoy. In: Ocean wave spectra. 1961, p. 111–32. URL: https://books.google.no/books/about/Ocean_wave_spectra.html?id=D1JVAAAAMAAJ&pgis=1.

[23] Mitsuyasu H, Tasai F, Suhara T, Mizuno S, Ohkusu M, Honda T, et al. Observations of the Directional Spectrum of Ocean Waves Using a Cloverleaf Buoy. J Phys Oceanogr 1975;5(4):750–60. URL: http://journals.ametsoc.org/doi/abs/10.1175/1520-0485(1975)005%3C0750:OOTDSO%3E2.0.CO;2. doi:10.1175/1520-0485(1975)005<0750:OOTDSO>2.0.CO;2.

[24] Hasselmann DE, Dunckel M, Ewing JA. Directional Wave Spectra Observed during JONSWAP 1973. J Phys Oceanogr 1980;10(8):1264–80. URL: http://journals.ametsoc.org/doi/abs/10.1175/1520-0485(1980)010%3C1264:DWSODJ%3E2.0.CO;2. doi:10.1175/1520-0485(1980)010<1264:DWSODJ>2.0.CO;2.

[25] WAMIT Inc. . WAMIT User Manual - Version 7.1. 2015. URL: www.wamit.com.

[26] DNV . SESAM User Manual Wadam Wave Analysis by Diffraction and Morison Theory. 2014.

[27] Henrici P. Fast Fourier methods in computational complex analysis. Siam Rev 1979;21(4):481–527. URL: http://epubs.siam.org/doi/abs/10.1137/1021093. doi:10.1137/1021093.

[28] Kress R. Numerical Analysis; vol. 181 of *Graduate Texts in Mathematics*. New York, NY: Springer New York; 1998. ISBN 978-1-4612-6833-8. URL: http://link.springer.com/10.1007/978-1-4612-0599-9. doi:10.1007/978-1-4612-0599-9.

[29] The MathWorks Inc. . MATLAB Release 2015a. 2015.

[30] Weideman J. Numerical integration of periodic functions: A few examples. Am Math Mon 2002;109(1):21–36. URL: http://www.jstor.org/stable/2695765. doi:10.2307/2695765.

[31] Shinozuka M. Monte Carlo solution of structural dynamics. Comput Struct 1972;2(5-6):855–74. URL: http://www.sciencedirect.com/science/article/pii/0045794972900430. doi:10.1016/0045-7949(72)90043-0.

[32] Opgård B, Allievi F. Chained Floating Bridge. In: IABSE Symposium Report; vol. 102. International Association for Bridge and Structural Engineering; 2014, p. 1236–43. URL: http://www.ingentaconnect.com/content/iabse/report/2014/00000102/00000021/art00007. doi:10.2749/222137814814067491.

[33] Koepf W. Hypergeometric Summation. Universitext; London: Springer London; 2014. ISBN 978-1-4471-6463-0. URL: http://link.springer.com/10.1007/978-1-4471-6464-7. doi:10.1007/978-1-4471-6464-7.

Appendix A.

This section includes the derivation of the expression for the cross-spectral density of the wave elevation given in Section 2.1. This derivation can also be found in [9].

When it is modelled as a homogeneous stationary stochastic process, the sea elevation at the point (x, y) at time t, denoted $\eta(x, y, t)$, is written as

$$\eta\left(x,y,t\right)=\int_{-\infty}^{\infty}e^{i\omega t-i\kappa(x\cos\theta+y\sin\theta)}dB\left(\boldsymbol{\kappa},\omega\right), \tag{A.1}$$

where $\boldsymbol{\kappa}=[\kappa\cos\theta,\kappa\sin\theta]$ is the wave number vector, ω is the frequency and $B\left(\boldsymbol{\kappa},\omega\right)$ is the spectral process associated with the wave elevation. The assumption of homogeneity and stationarity implies that the spectral process must have zero mean and orthogonal increments, giving the cross-correlation function

$$\begin{aligned}R_{mn}\left(\tau\right)&=E\left[\eta\left(x_m,y_m,t+\tau\right)\overline{\eta\left(x_n,y_n,t\right)}\right]\\&=\int_{-\infty}^{\infty}\int_{\theta}\int_{\kappa}e^{i\omega\tau}e^{-i\kappa(\Delta x\cos\theta+\Delta y\sin\theta)}S_{\eta\eta}^{(3)}\left(\kappa,\theta,\omega\right)d\kappa d\theta d\omega.\end{aligned} \tag{A.2}$$

Here $\Delta x=x_m-x_n$ and $\Delta y=y_m-y_n$ is the separation of the locations (x_m,y_m) and (x_n,y_n) in space and $S_{\eta\eta}^{(3)}\left(\kappa,\theta,\omega\right)$ is the three-dimensional wave spectral

density. The cross-spectral density is obtained as the Fourier transform of the cross-correlation function (A.2) with respect to the time lag τ:

$$\begin{aligned} S_{mn}(\omega) &= \frac{1}{2\pi}\int_{-\infty}^{\infty} R_{mn}(\Delta x, \Delta y, \tau)\, e^{-i\omega\tau} d\tau \\ &= \int_{\theta}\int_{\kappa} e^{-i\kappa(\Delta x\cos\theta + \Delta y \sin\theta)} S^{(3)}_{\eta\eta}(\kappa, \theta, \omega)\, d\kappa d\theta. \end{aligned} \tag{A.3}$$

The formula for the cross-spectral density can be simplified using the dispersion relation which relates the frequency ω and the wave number κ by a one-to-one mapping $\kappa = \kappa(\omega)$, or equivalently $\omega = \omega(\kappa)$. Now κ and ω are no longer independent variables in the integration in (A.3) and the formula finally reduces to

$$S_{mn}(\omega) = \int_{\theta} e^{-i\kappa(\omega)(\Delta x\cos\theta + \Delta y\sin\theta)} S^{(2)}_{\eta\eta}(\theta, \omega)\, d\theta,$$

where $S^{(2)}_{\eta\eta}(\theta, \omega)$ is the directional wave spectral density.

Appendix B.

This section is devoted to proving the identity (15), which is stated in Theorem 1 below. The proof of Theorem 1 relies upon two parts, which we summarize in two propositions.

Proposition 1. *For $n \in \{1, 2, 3, \dots\}$ and $\phi \in \mathbb{R}$ we have the following Fourier series expansions for even- and odd-numbered powers of the cosine function respectively:*

$$\cos^{2n}\phi = \frac{1}{2^{2n}}\binom{2n}{n} + \frac{1}{2^{2n-1}}\sum_{k=1}^{n}\binom{2n}{n+k}\cos(2k\phi) \tag{B.1a}$$

$$\cos^{2n-1}\phi = \frac{1}{2^{2n-2}}\sum_{k=1}^{n}\binom{2n-1}{n+k-1}\cos((2k-1)\phi) \tag{B.1b}$$

Proof. For $\tilde{n} \in \mathbb{N}$ we can use the complex representation of the cosine function

and the binomial theorem to obtain

$$\begin{aligned}
\cos^{\tilde{n}}\phi &= \frac{1}{2^{\tilde{n}}}\left(e^{i\phi}+e^{-i\phi}\right)^{\tilde{n}} = \frac{1}{2^{\tilde{n}}}\sum_{k=0}^{\tilde{n}}\binom{\tilde{n}}{k}e^{i(\tilde{n}-k)\phi}e^{-ik\phi} \\
&= \frac{1}{2^{\tilde{n}}}\sum_{k=0}^{\tilde{n}}\binom{\tilde{n}}{k}\left(\cos\left(\tilde{n}-k\right)\phi + i\sin\left(\tilde{n}-k\right)\phi\right)\left(\cos k\phi - i\sin k\phi\right) \\
&= \frac{1}{2^{\tilde{n}}}\sum_{k=0}^{\tilde{n}}\binom{\tilde{n}}{k}\left(\cos\left(\tilde{n}-k\right)\phi\cos k\phi + \sin\left(\tilde{n}-k\right)\phi\sin k\phi\right) \\
&\quad + i\frac{1}{2^{\tilde{n}}}\sum_{k=0}^{\tilde{n}}\binom{\tilde{n}}{k}\left(\sin\left(\tilde{n}-k\right)\phi\cos k\phi - \cos\left(\tilde{n}-k\right)\phi\sin k\phi\right) \\
&= \frac{1}{2^{\tilde{n}}}\sum_{k=0}^{\tilde{n}}\binom{\tilde{n}}{k}\cos\left(\left(\tilde{n}-2k\right)\phi\right) - i\frac{1}{2^{\tilde{n}}}\sum_{k=0}^{\tilde{n}}\binom{\tilde{n}}{k}\sin\left(\left(\tilde{n}-2k\right)\phi\right).
\end{aligned}$$

Assuming $\phi \in \mathbb{R}$ it is obvious that $\cos^{\tilde{n}}\phi$ is a real number, which means that the imaginary part of the right hand side above must vanish, resulting in the expression

$$\cos^{\tilde{n}}\phi = \frac{1}{2^{\tilde{n}}}\sum_{k=0}^{\tilde{n}}\binom{\tilde{n}}{k}\cos\left(\left(\tilde{n}-2k\right)\phi\right). \tag{B.2}$$

If $\tilde{n}$ is an even number it can be written as $\tilde{n} = 2n$ for some $n \in \{1, 2, 3, \dots\}$ and we have then

$$\cos^{2n}\phi = \frac{1}{2^{2n}}\sum_{k=0}^{2n}\binom{2n}{k}\cos\left(2\left(n-k\right)\phi\right). \tag{B.3}$$

For the binomial coefficients we have the symmetry property

$$\binom{2n}{2n-k} = \binom{2n}{k}, \qquad\qquad k \in \{0, 1, 2, \dots, 2n\}, \tag{B.4}$$

which along with the symmetry of the cosine function gives that term number $2n-k$ in the sum (B.3) is equal to term number k. Thus each term is repeated twice, except for the middle term where $k = n$, and the sum can be written as

$$\begin{aligned}
\cos^{2n}\phi &= \frac{1}{2^{2n}}\binom{2n}{n} + \frac{1}{2^{2n-1}}\sum_{k=0}^{n-1}\binom{2n}{k}\cos\left(2\left(n-k\right)\phi\right) \\
&= \frac{1}{2^{2n}}\binom{2n}{n} + \frac{1}{2^{2n-1}}\sum_{k=1}^{n}\binom{2n}{n-k}\cos\left(2kx\right),
\end{aligned}$$

where the last equality is simply a reordering of the terms. Finally (B.1a) is obtained by again using the symmetry property (B.4) of the binomial coefficient.

If on the other hand $\tilde{n}$ is an odd number in (B.2) we can write $\tilde{n} = 2n - 1$ for some $n \in \{1, 2, 3, \dots\}$, and (B.1b) is obtained using the same approach as for even $\tilde{n}$, observing that two and two terms are equal.

Proposition 2. *For $k \in \{0, 1, 2, 3, \dots\}$ and $s \in \mathbb{R}$ with $s \geq 0$ the following holds:*

$$\sum_{n=0}^{\infty} \frac{1}{2^{2n+k-1}} \binom{s}{2n+k} \binom{2n+k}{n+k} = \frac{1}{2^{s-1}} \binom{2s}{s+k}. \tag{B.5}$$

Here the binomial coefficients are interpreted in the generalized sense, being defined using the gamma function by

$$\binom{a}{b} = \frac{\Gamma(a+1)}{\Gamma(a-b+1)\Gamma(b+1)}, \qquad a, b \in \mathbb{R}.$$

Proof. The key for calculating the series is the method of hypergeometric summation [33]. First we use Algorithm 2.8 in [33] to write the series in (B.5) as a hypergeometric function. Expressing the binomial coefficients using the gamma function, the n-th term in the series can be written as

$$a_n = \frac{1}{2^{2n+k-1}} \binom{s}{2n+k} \binom{2n+k}{n+k} = \frac{1}{2^{2n+k-1}} \frac{\Gamma(s+1)}{\Gamma(s-2n-k+1)\, n!\, (n+k)!}.$$

This gives the term ratio

$$\frac{a_{n+1}}{a_n} = \frac{(s-2n-k)(s-2n-k-1)}{4(n+1)(n+k+1)} = \frac{\left(n+\frac{k-s}{2}\right)\left(n+\frac{k+1-s}{2}\right)}{(n+1)(n+k+1)},$$

where we have used the property that $\Gamma(x+1) = x\Gamma(x)$ for any x. Thus the term ratio is written as $\frac{a_{n+1}}{a_n} = \frac{u_n}{v_n}$, where u_n and v_n are polynomials in n factorized in linear factors. Observing that the initial term is

$$a_0 = \frac{1}{2^{k-1}} \frac{\Gamma(s+1)}{\Gamma(s-k+1)\, k!} = \frac{1}{2^{k-1}} \binom{s}{k},$$

it follows from Algorithm 2.8 in [33] that we can rewrite the series using the Gauss hypergeometric series as

$$\sum_{n=0}^{\infty} \frac{1}{2^{2n+k-1}} \binom{s}{2n+k} \binom{2n+k}{n+k} = \frac{1}{2^{k-1}} \binom{s}{k} {}_2F_1\left(\frac{k-s}{2}, \frac{k+1-s}{2}; k+1; 1\right). \tag{B.6}$$

The Gauss hypergeometric series is defined as

$${}_2F_1(a, b; c; z) = \frac{\Gamma(c)}{\Gamma(a)\Gamma(b)} \sum_{n=0}^{\infty} \frac{\Gamma(a+n)\Gamma(b+n)}{\Gamma(c+n)} \frac{z^n}{n!},$$

and according to property 15.1.20 in [21] we have for $z = 1$ that

$${}_2F_1(a, b; c; 1) = \frac{\Gamma(c)\Gamma(c-a-b)}{\Gamma(c-a)\Gamma(c-b)}$$

holds whenever $\mathrm{Re}(c-a-b) > 0$ and $c \notin \{0, -1, -2, -3, \dots\}$. Using this property (B.6) yields

$$\sum_{n=0}^{\infty} \frac{1}{2^{2n+k-1}} \binom{s}{2n+k} \binom{2n+k}{n+k} = \frac{1}{2^{k-1}} \binom{s}{k} \frac{\Gamma(k+1)\Gamma\left(s+\frac{1}{2}\right)}{\Gamma\left(\frac{s+k+2}{2}\right)\Gamma\left(\frac{s+k+1}{2}\right)}, \tag{B.7}$$

which is valid for $\mathrm{Re}\left(k+1-\frac{k-s}{2}-\frac{k+1-s}{2}\right)=\mathrm{Re}(s)+\frac{1}{2}>0$ and $k\notin\{-1,-2,-3,\dots\}$. These conditions are clearly satisfied when $s\in\mathbb{R}$ with $s\geq 0$ and $k\in\{0,1,2,3,\dots\}$. Finally we rewrite the expression obtained in (B.7) using property 6.1.18 in [21], the duplication formula for the gamma function, finding that

$$\begin{aligned}\sum_{n=0}^{\infty}\frac{1}{2^{2n+k-1}}\binom{s}{2n+k}\binom{2n+k}{n+k}&=\frac{2^{s+1}\Gamma\left(s+\frac{1}{2}\right)\Gamma(k+1)}{\sqrt{\pi}\Gamma(s+k+1)}\binom{s}{k}\\&=\frac{2^{s+1}\Gamma\left(s+\frac{1}{2}\right)\Gamma(k+1)\Gamma(s+1)}{\sqrt{\pi}\Gamma(s+k+1)\Gamma(s-k+1)\Gamma(k+1)}\\&=\frac{1}{2^{s-1}}\frac{\Gamma(2s+1)}{\Gamma(s+k+1)\Gamma(s-k+1)}\\&=\frac{1}{2^{s-1}}\binom{2s}{s+k},\end{aligned}$$

which concludes the proof.

With the aid of Proposition 1 and Proposition 2 we can now prove the identity (15) which we state here as a Theorem.

Theorem 1. *Let s be any non-negative real number. Then for any $\phi\in\mathbb{R}$ the following equality holds:*

$$\begin{aligned}\left(\cos^2\frac{\phi}{2}\right)^s&=\frac{1}{2^{2s}}\binom{2s}{s}+\frac{1}{2^{2s-1}}\sum_{k=1}^{\infty}\binom{2s}{s+k}\cos(k\phi)\\&=\frac{1}{2^{2s}}\frac{\Gamma(2s+1)}{\Gamma^2(s+1)}+\frac{1}{2^{2s-1}}\sum_{k=1}^{\infty}\frac{\Gamma(2s+1)}{\Gamma(s-k+1)\Gamma(s+k+1)}\cos(k\phi).\end{aligned}$$

Proof. Let s be any non-negative real number and define the function $f:\mathbb{R}\to\mathbb{R}$ by

$$f(\phi)=\left(\cos^2\frac{\phi}{2}\right)^s=\frac{1}{2^s}(1+\cos\phi)^s,\qquad\qquad\phi\in\mathbb{R}.$$

Now $f(\phi)$ can be expanded using the binomial series as

$$f(\phi)=\frac{1}{2^s}\sum_{n=0}^{\infty}\binom{s}{n}\cos^n\phi,\tag{B.8}$$

which is convergent for any value of ϕ, since $s\geq 0$. In order to further expand $f(\phi)$ into a Fourier series we split the series (B.8) into two series of even and odd powers of the cosine function respectively, and utilize the formulas (B.1a)

and (B.1b) from Proposition 1. This yields

$$\begin{aligned}
2^s f(\phi) &= 1 + \sum_{n=1}^{\infty} \binom{s}{2n} \cos^{2n}\phi + \sum_{n=1}^{\infty} \binom{s}{2n-1} \cos^{2n-1}\phi \\
&= 1 + \sum_{n=1}^{\infty} \frac{1}{2^{2n}} \binom{s}{2n} \binom{2n}{n} + \sum_{n=1}^{\infty} \sum_{k=1}^{n} \frac{1}{2^{2n-1}} \binom{s}{2n} \binom{2n}{n+k} \cos(2k\phi) \\
&\quad + \sum_{n=1}^{\infty} \sum_{k=1}^{n} \frac{1}{2^{2n-2}} \binom{s}{2n-1} \binom{2n-1}{n+k-1} \cos((2k-1)\phi).
\end{aligned}$$

Changing the order of summation gives

$$\begin{aligned}
2^s f(\phi) &= \frac{1}{2} \sum_{n=0}^{\infty} \frac{1}{2^{2n-1}} \binom{s}{2n} \binom{2n}{n} + \sum_{k=1}^{\infty} \left(\sum_{n=k}^{\infty} \frac{1}{2^{2n-1}} \binom{s}{2n} \binom{2n}{n+k} \right) \cos(2k\phi) \\
&\quad + \sum_{k=1}^{\infty} \left(\sum_{n=k}^{\infty} \frac{1}{2^{2n-2}} \binom{s}{2n-1} \binom{2n-1}{n+k-1} \right) \cos((2k-1)\phi),
\end{aligned}$$

and if we change the summation index such that all sums start from $n = 0$ we obtain

$$\begin{aligned}
2^s f(\phi) &= \frac{1}{2} \sum_{n=0}^{\infty} \frac{1}{2^{2n-1}} \binom{s}{2n} \binom{2n}{n} + \sum_{k=1}^{\infty} \left(\sum_{n=0}^{\infty} \frac{1}{2^{2n+2k-1}} \binom{s}{2n+2k} \binom{2n+2k}{n+2k} \right) \cos(2k\phi) \\
&\quad + \sum_{k=1}^{\infty} \left(\sum_{n=0}^{\infty} \frac{1}{2^{2n+2k-2}} \binom{s}{2n+2k-1} \binom{2n+2k-1}{n+2k-1} \right) \cos((2k-1)\phi) \\
&= \frac{1}{2} \sum_{n=0}^{\infty} \frac{1}{2^{2n-1}} \binom{s}{2n} \binom{2n}{n} + \sum_{k=1}^{\infty} \left(\sum_{n=0}^{\infty} \frac{1}{2^{2n+k-1}} \binom{s}{2n+k} \binom{2n+k}{n+k} \right) \cos(k\phi),
\end{aligned}$$

where the last equality is obtained by combining the sums with even and odd indices. Finally the Fourier coefficients are found by computing the series according to Proposition 2 and we end up with

$$\begin{aligned}
\left(\cos^2\frac{\phi}{2}\right)^s &= \frac{1}{2^{2s}} \binom{2s}{s} + \frac{1}{2^{2s-1}} \sum_{k=1}^{\infty} \binom{2s}{s+k} \cos(k\phi) \\
&= \frac{1}{2^{2s}} \frac{\Gamma(2s+1)}{\Gamma^2(s+1)} + \frac{1}{2^{2s-1}} \sum_{k=1}^{\infty} \frac{\Gamma(2s+1)}{\Gamma(s-k+1)\,\Gamma(s+k+1)} \cos(k\phi),
\end{aligned}$$

which is what we wanted to prove.